
Effective Model Sparsification by Scheduled Grow-and-Prune Methods

Xiaolong Ma^{1,2,†}, Minghai Qin^{1,†,‡}, Fei Sun^{1,†}, Zejiang Hou^{1,3}, Kun Yuan¹, Yi Xu¹, Yanzhi Wang², Yen-Kuang Chen¹, Rong Jin¹, and Yuan Xie¹

¹ DAMO Academy, Alibaba Group

² Northeastern University

³ Princeton University

Abstract

Deep neural networks (DNNs) are effective in solving many real-world problems. Larger DNN models usually exhibit better quality (e.g., accuracy) but their excessive computation results in long training and inference time. Model sparsification can reduce the computation and memory cost while maintaining model quality. Most existing sparsification algorithms unidirectionally remove weights, while others randomly or greedily explore a small subset of weights in each layer for pruning. The limitations of these algorithms reduce the level of sparsity. In addition, many algorithms still require pre-trained dense models and thus suffer from large memory footprint. In this paper, we propose a novel scheduled grow-and-prune (GaP) methodology without having to pre-train a dense model. It addresses the shortcomings of the previous work by repeatedly growing a subset of layers to dense and then pruning them back to sparse after some training. Experiments have shown that such models can match or beat the quality of highly optimized dense models at 80% sparsity on a variety of tasks, such as image classification, objective detection, 3D object part segmentation, and translation. They also outperform other state-of-the-art (SOTA) methods for model sparsification. As an example, a 90% sparse ResNet-50 obtained via GaP achieves 77.9% top-1 accuracy on ImageNet, improving the SOTA results of sparsification algorithms by 1.5%.

1 Introduction

Deep neural networks (DNNs) have achieved great performance in many real-world scenarios. However, the large computation and memory requirements of deep neural networks discourage them from being applied to broader applications on resource-limited devices. Model compression via weight pruning is a popular research topic, where a large proportion of weights are set to zero, leading to significant reduction in both memory and computation. The introduction of sparse tensor cores in the NVIDIA A100 GPU [1] brings the sparsity-based model compression into mainstream.

Early works on weight pruning generally follow a **prune-from-dense** methodology [2, 3, 4, 5, 6, 7, 8, 9], which usually requires 3 phases of training: pre-train a dense model, prune it to sparse, and fine-tune it. In such methodologies, however, the pre-trained dense models consume large memory space and may lead to long training time. In addition, one-shot or iteratively pruning from a well-trained DNN can only *remove* weights, which lacks the flexibility of growing back weights that are considered unimportant early in the training process but showed to be significant later in training.

† Equal contribution.

‡ minghai.qin@alibaba-inc.com

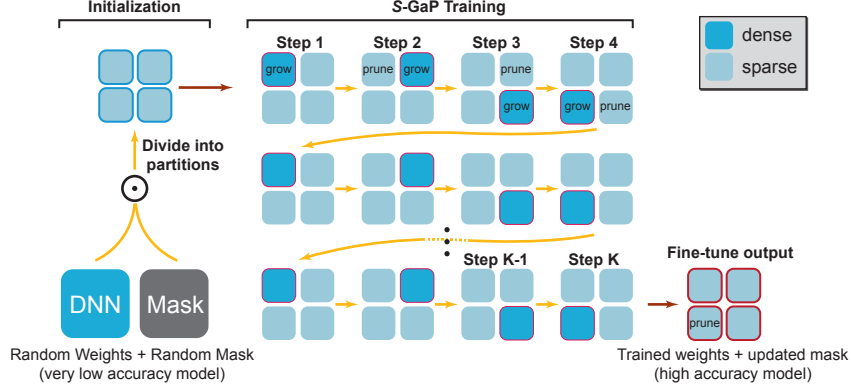


Figure 1: Overview of the sequential GaP (S-GaP) training method. We assume 4 partitions in a model are grown and pruned in a cyclic order. Only one partition is kept dense during training. After K steps, the dense partition is pruned and the whole model is fine-tuned to obtain the sparse model.

Table 1: Comparison of model sparsification methods.

Method	Dense Pre-training	Mask exploration	Evaluated applications	Model quality
Prune-from-dense	Yes	No	All	Better
Early-stage pruning	Partial	No	CV(2D)	Good
Existing mask exploration	No	Random/Greedy	CV(2D), NLP	Better
Scheduled GaP (Ours)	No	Scheduled	CV(2D,3D), NLP	Best

On the other hand, **early-stage pruning** methods [10, 11, 12] avoid training dense models to converge. However, those sparse masks are prematurely fixed, resulting in inferior model quality.

Methods based on **sparse mask exploration**, such as DeepR [13], SET [14], DSR [15], and RigL [16] maintain the target sparsity in all layers throughout the training process and selectively explore a small fraction of the weights periodically. The explored weights are chosen based on random or greedy heuristics, leading to limited coverage of sparse patterns and consequentially sub-optimal performance.

In order to overcome the shortcomings of the previous solutions, we propose a scheduled grow-and-prune (GaP) methodology. It does not require a dense model any time during the training process, leading to largely-reduced memory footprints. Meanwhile, the sparse mask of a layer is updated after exploring all weights in the same layer, resulting in better mask-update efficiency.

The scheduled GaP methodology divides a randomly initialized DNN with random sparse masks into κ partitions. The sparse mask of a partition is updated by first growing the partition to a dense one, updating the weights in the dense partition with some amount of training, and then pruning it back to a sparse partition. If the mask for each partition is processed one by one, it is called the *sequential* GaP method (as shown in Figure 1). If the masks for all partitions are processed at the same time in different machines, it is called the *parallel* GaP method. Such a process is carefully scheduled to ensure that the weights in all layers are periodically explored to update the sparse masks. The proposed methods also enable continuous evolving of sparse masks without the need to pre-determine the number of training epochs, resulting in better quality of the sparse models.

The differences between our proposed methods and the previous methods are summarized in Table 1. Our methods outperform previous methods over a wide variety of applications. The quality comparison is based on the best results on the ResNet-50 models at 80% and 90% sparsity. In addition, we illustrate the difference from existing mask exploration methods by an example in Figure 2. In the scheduled GaP methods, all weights to be grown (or to be pruned) belong to the same partition. Since each layer is grown to dense at least once, all weights in the model are guaranteed to be explored. On the other hand, in the random or greedy exploration methods, the grown and pruned weights are distributed across all layers and they do not guarantee that all weights are explored, e.g., the connection between 1st input neuron and 3rd neuron in the first layer is not explored in Figure 2(b).

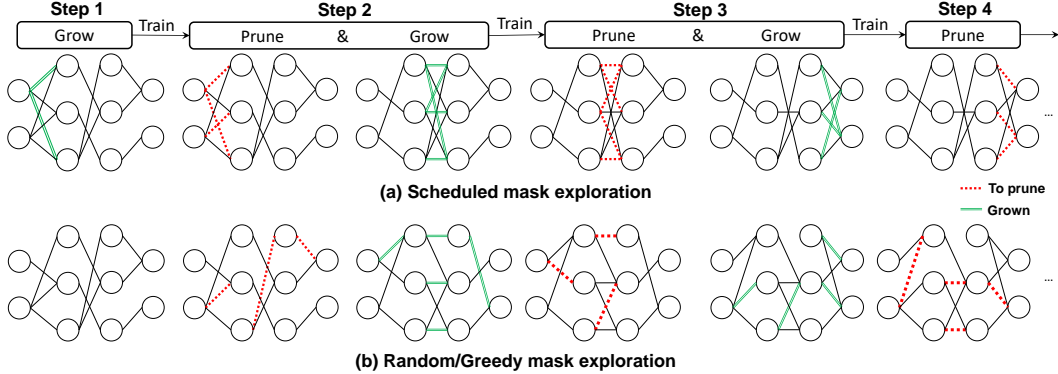


Figure 2: Comparison between (a) the scheduled mask exploration and (b) the random/greedy mask exploration. In (a), the weights to be grown (or pruned) are in the same layer and the growing phase covers all weights in that layer; In (b), they can be in different layers and the growing phase does not guarantee a coverage during training.

The contribution of this paper is summarized as follows.

- We propose two GaP methods such that they do not require to train a dense model any time throughout the training process, reducing the training memory footprints.
- Sparse models obtained by the proposed GaP methods outperform the SOTA sparsification algorithms on a wide variety of deep learning tasks, including 2D image recognition, object detection, 3D object part segmentation, and machine translation.
- For all four tasks, the proposed GaP methods surprisingly generate sparse models that match or even exceed the dense counterparts at 80% sparsity.
- We provide theoretical guarantees for the GaP method and clarify its convergence property. In particular, we justify the influence of the mask-induced error.

2 Methodology

In this section, we describe the scheduled grow-and-prune (GaP) methods in detail.

Figure 1 illustrates the sequential GaP method. Assume a DNN is divided into κ partitions ($\kappa = 4$ in Figure 1) and the choice of the dense partition rotates among all κ partitions. Starting from all partitions with random sparse masks, the first partition is grown to a dense one. All weights in the first partition and the masked weights in the remaining 3 partitions are trained for a few epochs (Step 1). Then the first partition is pruned to sparse (Step 2). Next, we apply the same strategy to the second partition, then continue iterating over all κ partitions. This process is repeated K times. Finally, the last dense partition is pruned and the model is fine-tuned to obtain a fully sparse model.

As a natural extension, we also propose a *parallel* GaP method to accelerate the wall-clock training time using multiple nodes (e.g. machines). It distributes the same fully-sparse model to several nodes. Each node grows one different partition to dense and trains it for a few epochs. Then the dense partitions are combined into a dense model in a central node, though no training is required. Finally, the dense model is pruned and re-distributed for another step of parallel GaP.

2.1 Grow-and-prune unit

A deep neural network model can be written as $f(x; \Theta)$, where $\Theta \in \mathbb{R}^M$ are M trainable weights and x are training samples. We can train it with a binary mask $m \in \{0, 1\}^M$, where a zero in m means that the corresponding weight in Θ is fixed to be zero and a one in m means that the corresponding weight in Θ is free to be updated. Therefore, a sparse weight tensor can be represented as $\Theta \odot m$, where \odot denotes element-wise multiplication. The corresponding model with the mask is denoted as $f(x; \Theta \odot m)$.

Algorithm 1: S-GaP training flow.

Input: An L -layer model with uninitialized weight Θ ; pruning ratio r .
Output: An L -layer sparse model satisfying the target sparsity requirement.
Divide all layers into κ partitions, denoted by $S_i, \forall i \in \{1, 2, \dots, \kappa\}$.
Initialize $f(x; \Theta \odot m)$ with random weights Θ and random masks m that satisfy the sparsity requirement.
 $step = 1$
while $step \leq K$ **do**
 if there exists a dense S_i **then**
 Prune Θ^{S_i} and update m^{S_i} by $[\Theta^{S_i}, m^{S_i}] \leftarrow \text{ArgPruneTo}(\Theta^{S_i}, r)$.
 Select a sparse partition S_j other than S_i , and update the corresponding mask m^{S_j} as an all-one mask for the S_j partition by $m^{S_j} \leftarrow \text{ArgGrowTo}(\Theta^{S_j})$.
 Train the model $f(x; \Theta \odot m)$ for T epochs.
 $step = step + 1$
 Denote the final dense partition by S_d .
 Prune Θ^{S_d} and update m^{S_d} by $[\Theta^{S_d}, m^{S_d}] \leftarrow \text{ArgPruneTo}(\Theta^{S_d}, r)$.
 Fine-tune $f(x; \Theta \odot m)$ for T' epochs.

We use superscript to denote a subset of Θ and m . That is, Θ^S and m^S denote a subset of trainable weights and their masks, respectively. Suppose the model $f(\cdot)$ contains L layers, and let κ be an integer between 1 and L and the set $\{1, 2, \dots, L\}$ be divided into κ subset $S_1, S_2, \dots, S_\kappa$. Consequently, Θ is divided into κ partitions, denoted as $\Theta^{S_1}, \dots, \Theta^{S_\kappa}$. For the i -th partition Θ^{S_i} , we denote its mask by m^{S_i} .

The GaP method trains each partition Θ^{S_i} in two phases. One phase is the sparse training after weight pruning. The pruning operation is defined as $[\Theta^{S_i}, m^{S_i}] \leftarrow \text{ArgPruneTo}(\Theta^{S_i}, r)$. It finds the sparse mask m^{S_i} based on certain criteria (e.g., magnitude-based pruning) on the partition Θ^{S_i} with a pruning ratio r , and then prunes the weights by $\Theta^{S_i} \leftarrow \Theta^{S_i} \odot m^{S_i}$. The other phase is the dense training after weight growing. The growing operation is defined as $m^{S_i} \leftarrow \text{ArgGrowTo}(\Theta^{S_i})$. It sets the mask m^{S_i} to be all-one such that all weights Θ^{S_i} are free to be updated during training. Note that $\text{ArgGrowTo}(\Theta^{S_i})$ only resets the mask. Therefore, some of the weights in Θ^{S_i} are zeros after performing $\text{ArgGrowTo}(\Theta^{S_i})$ and they may be updated to non-zero values during training. Note that these two operations do not require any training, they only prune Θ and update m once. After calling these two operations, the models are trained with a mask where only the weights corresponding to the mask values of one may be updated in the back-propagation, and the rest of the weights remain zero until the next call to these operations.

2.2 Sequential GaP

In this section, we use the GaP unit to design the sequential Gap (S-GaP) sparse training framework as depicted in Figure 1. The chosen partitions for growing and pruning rotate in the sequential order as Algorithm 1 describes.

If κ partitions follow a natural order of layers and if $j = i + 1$ (when $i < \kappa$) or $j = 1$ (when $i = \kappa$), we call the GaP *cyclic-partitioned*. When all layers are cyclically grown and pruned once after κ steps, we call it *one round*.

The GaP process starts with random weights and masks, maintaining only one dense partition throughout training. It does not require training a dense model to obtain the sparse mask. In the process, only the weights for convolution, matrix-vector, and matrix-matrix multiplications are made sparse. The weights related to biases and batch-normalization are kept dense, as they are critical for model quality but only contribute to a tiny fraction of the inference FLOPs.

2.3 Parallel GaP

In this section, we introduce the parallel GaP (*P*-GaP) as a flexible and highly efficient complement to the S-GaP sparse training method when sufficient training resources are available. Unlike the S-GaP where partitions are grown and pruned serially in one machine, the *P*-GaP distributes the model to κ machines. Each grows a different partition to dense and trains the model in parallel. The trained dense partitions are combined to a dense model and pruned to a sparse one again. Each pair

Algorithm 2: *P*-GaP training flow.

Input: An L -layer model with uninitialized weight Θ ; pruning ratio r .
Output: An L -layer sparse model satisfying the target sparsity requirement.
Divide all layers into κ partitions, denoted by $S_i, \forall i \in \{1, 2, \dots, \kappa\}$.
Initialize $f(x; \Theta \odot m)$ with random weights Θ and random masks m that satisfy the sparsity requirement.
 $step = 1$
while $step \leq K$ **do**
 Send identical copies of $[\Theta, m]$ to all κ nodes and denote them by $\Theta(i)$ and $m(i)$ on the i -th node.
 parfor $i \in \{1, \dots, \kappa\}$ **do**
 Grow S_i by updating the mask $m(i)^{S_i} \leftarrow \text{ArgGrowTo}(\Theta(i)^{S_i})$.
 Train the model $f(x; \Theta(i) \odot m(i))$ for T epochs.
 Collect the dense partition $\Theta(i)^{S_i}$ from the i -th machine.
 Combine all $\Theta(i)^{S_i}$ into a dense model $\Theta^{S_1 \cup \dots \cup S_\kappa}$ with the updated weights.
 Prune Θ and update m by $[\Theta, m] \leftarrow \text{ArgPruneTo}(\Theta, r)$.
 $step = step + 1$.
Fine-tune $f(x; \Theta \odot m)$ for T' epochs.

of distribution and combining form one round in the *P*-GaP. Unlike *S*-GaP, one round *P*-GaP consists of only one step. The detailed *P*-GaP method is shown in Algorithm 2.

Some of the differences between the parallel GaP and the conventional distributed training are listed as follows.

1. In *P*-GaP, data communicates across different server nodes every T epochs of training. It is far less frequent than conventional distributed training, which requires communications and synchronization in every mini-batch. Therefore, the data bandwidth between the nodes can be kept at minimal.
2. In *P*-GaP, each node can use the single-node hyper-parameters to train the sparse models. It does not require excessively large batch-size to fully utilize the computing resource.
3. Different from data parallelism, model parallelism, and pipeline parallelism, the *P*-GaP explores another dimension of parallelism when training sparse models, which we call it *mask parallelism*. This implies that masks in different partitions are less correlated and can be searched separately.

3 Experimental Results

This section evaluates the proposed *S*-GaP and *P*-GaP sparse training methods on different machine learning tasks. Since our goal is to search for the optimal sparse models to speed up inference, we report the best model accuracy obtained using the GaP methods for all models.

All of our experimental results are trained and inference in the machines with 8 NVIDIA-V100 GPUs. The sequential GaP is trained in one training node and the parallel GaP is trained in κ training nodes, where κ is the number of model partitions. The training platform is PyTorch. In the pruning stage of the GaP method, the weights with the lowest magnitudes are pruned to zero. Most training scripts and hyper-parameters are inherited from [17] and [18]. Identical hyper-parameters are applied to each GaP step and the final fine-tune stage. For example, the initial learning rate of each step is restored to the same value. This hyper-parameter restoration avoids pre-determining the total number of epochs before training and enables the GaP methods to continuously search for sparse masks.

3.1 Image classification: ResNet-50 on ImageNet

In the image classification task, we use standard data augmentation, a batch size of 2048, cosine annealing learning rate schedule, SGD optimizer with a momentum of 0.875, and a weight decay of 3.05e-5. The learning rate is scheduled with a linear warm-up for 2 epochs before reaching the initial learning rate of 2.048. Each GaP step with non-uniform and uniform sparsity includes 30 of training, respectively. The final fine-tuning includes 150 epochs.

Table 2 compares the accuracy between using the GaP methods and other previous work. We evaluate the performance of both cyclic-partitioned *S*-GaP and *P*-GaP. The ResNet-50 is divided into four partitions by the last three downsampling stages. For non-uniform sparsity, all layers are sparsified.

Table 2: Results of sparse ResNet-50 models on ImageNet.

Method	Distribution	Sparsity ratio: 80%		Sparsity ratio: 90%	
		Top-1 Acc (%)	FLOPS ($\times 10^9$)	Top-1 Acc (%)	FLOPS ($\times 10^9$)
Dense [17]		Top-1 accuracy: 78.2, FLOPS: 8.2 $\times 10^9$			
Prune from Dense [19]	uniform	77.1	1.7	75.8	0.8
RigL [16]	uniform	74.6	1.7	72.0	0.8
RigL _{5x} [16]	uniform	76.6	1.7	75.7	0.8
S-GaP	uniform	77.9	1.7	76.3	0.8
P-GaP	uniform	77.5	1.7	76.1	0.8
SNIP [10]	non-uniform	69.7	2.8	61.9	1.9
GraSP [11]	non-uniform	72.1	2.8	68.1	1.9
DeepR [13]	non-uniform	71.7	n/a	70.2	n/a
SET [14]	non-uniform	72.6	1.7	70.4	0.8
DSR [15]	non-uniform	73.3	2.9	71.6	0.8
Prune w/ feedback [20]	non-uniform	75.1	n/a	n/a	n/a
RigL [16]	non-uniform (ERK)	75.1	3.4	73.0	2.0
RigL _{5x} [16]	non-uniform (ERK)	77.1	3.4	76.4	2.0
S-GaP	non-uniform	78.1	2.7	77.9	2.0

For the uniform sparsity, the first convolutional layer with 7×7 kernels is kept dense, the same as in [16]. The fully connected layer only contributes 0.5% of FLOPs, thus it is also kept dense. We report the accuracy of the best model searched within 100 GaP steps.

We observe that the improvement over [16] is 1.3% (77.9% vs. 76.6%) at 80% sparsity, and 0.6% (76.3% vs. 75.7%) at 90% sparsity. The **S-GaP** is also better than our re-implementation of the prune-from-dense method using ADMM [19]. For non-uniform sparse ResNet-50, the improvement over [16] is 1.0% (78.1% vs 77.1%) and 1.5% (77.9% vs. 76.4%) at 80% and 90% sparsity, respectively. Note that the 80% sparse ResNet-50 can almost match the accuracy of the dense model reported by NVIDIA [17].

3.2 Object detection: SSD on COCO-2017

To train SSD on COCO-2017 dataset, we use an input size of 300×300 pixels, a batch size of 64, step learning rate schedule, SGD optimizer with a momentum of 0.9, and a weight decay of 5e-4. The learning rate is 2.6e-3 with 300 iterations of linear warm-up. Each GaP step includes 32 epochs of training and the final fine-tuning includes 65 epochs.

We divide the SSD network into 4 partitions with three in the backbone and one in the detection head. We train the model using cyclic-partitioned **S-GaP** with a uniform weight sparsity of 90% on all layers except for the last output layer, which is kept dense. We report the accuracy of the best model searched within 40 GaP steps. As shown in Table 3, in the mean average precision category mAP@[.5:.95], the sparse model obtained using our **S-GaP** method exceeds the dense model by 0.7 mAP (25.9 vs 25.2). It also exceeds the best sparse model iteratively pruned from the dense model by 1.6 mAP (25.9 vs 24.3).

Table 3: Results of sparse SSD models for object detection on COCO-2017.

Method	Sparsity	AP, IoU:			AP, Area:			AR, #Dets:			AR, Area:		
		ratio	0.5:0.95	0.5	0.75	S	M	L	1	10	100	S	M
Dense [17]	0	25.2	42.7	25.8	7.3	27.1	40.8	23.8	34.5	36.1	11.7	39.6	56.1
Prune from dense	90%	24.3	41.1	24.8	6.8	26.3	40.0	23.3	34.0	35.8	11.1	39.4	55.7
S-GaP	90%	25.9	42.3	26.9	8.0	28.1	42.6	24.7	35.9	37.8	12.7	41.5	58.5

3.3 3D object part segmentation: PointNet++ on ShapeNet

When training PointNet++ [21, 18] model on ShapeNet [22] dataset, we use a batch size of 32, step learning rate schedule with an initial learning rate of 0.001, SGD optimizer with a momentum of 0.9,

and a weight decay of 1e-4. Each step of GaP includes 25 epochs of training. The final fine-tuning includes 250 epochs.

We divide the PointNet++ model into 4 partitions with three in the backbone and one in the segmentation head. We apply the *S*-GaP and *P*-GaP methods with uniform sparsity of 80% and 90% on all layers, respectively. We report the accuracy of the best model searched within 40 GaP steps. Table 4 compares them with the dense model and the best sparse model pruned from the dense model using the ADMM algorithm. The results show that on the class and instance mAP categories, the pruned model using the *S*-GaP method easily beats the model pruned from dense at both sparsities. It even beats the dense model at 80% sparsity. The pruned model using the *P*-GaP method also beats the model pruned from dense at 80% sparsity and is not far behind at 90% sparsity.

Table 4: Results of sparse PointNet++ models for 3D part segmentation on ShapeNet.

Method	#Points	Sparsity ratio: 80%		Sparsity ratio: 90%	
		Class mIoU (%)	Instance mIoU (%)	Class mIoU (%)	Instance mIoU (%)
Dense [18]	2k	Class mIoU: 82.5, Instance mIoU: 85.4			
prune from dense	2k	79.1	84.5	77.1	84.0
<i>S</i>-GaP	2k	82.9	85.8	79.5	85.1
<i>P</i>-GaP	2k	80.8	85.5	74.0	83.7

3.4 Translation: Transformer on WMT-14 En-De dataset

In this part, we evaluate the *S*-GaP and the *P*-GaP methods on the translation task based on Transformer [23]. We train the Transformer models on the WMT-14 En-De dataset and evaluate the SacreBLEU score [24].

We use a batch size of 5120, inverse square-root scheduler with an initial learning rate of 0.000846, and Adam optimizer. Each step in GaP includes 10 epochs of training, and the final fine-tuning includes 40 epochs.

We equally divide the Transformer models into three or six partitions with the decoder containing $2 \times$ partitions of the encoder. We apply the *S*-GaP and *P*-GaP methods with uniform sparsity of 80% and 90% on all layers, respectively.

We report the best SacreBLEU scores on the validation dataset in Table 5 within 30 GaP steps. The models trained using both *S*-GaP and *P*-GaP methods significantly improve over the sparse models obtained by pruning from the dense counterparts. They exceed the dense model quality at 80% sparsity, and the model using three-partition *S*-GaP method even outperforms the dense model at 90% sparsity.

Table 5: Results of sparse Transformer models for the translation task on WMT14 En-De.

Method	Sparsity ratio: 80%		Sparsity ratio: 90%	
	$\kappa = 3$	$\kappa = 6$	$\kappa = 3$	$\kappa = 6$
Dense [17]	SacreBLEU: 27.6			
Prune from dense	27.1		25.7	
<i>S</i>-GaP	27.6	27.6	27.7	27.1
<i>P</i>-GaP	27.9	27.7	27.3	26.9

4 Ablation Study

In this section, we present some ablation study on the proposed GaP methods.

4.1 Number of partitions for GaP

The number of partitions in GaP methods play a key role in obtaining better results. As compared in Table 6 and Table 7, one partition is not sufficient to preserve the best quality. Too many partitions

may reduce quality as well (as shown in the model with six partitions in Table 7). Empirically, a small number of equal partitions that naturally follow the structures of the models usually perform well. For example, ResNet-50 model is composed of four blocks, each sub-samples from the previous block. Thus a four-partition GaP is a natural choice. Transformer model contains an encoder and a decoder, with the decoder twice the number of attention blocks as the encoder. It is naturally divided to three partitions.

Table 6: The effect of different number of partitions for ResNet-50 models on ImageNet.

Method	Sparsity Ratio	Distribution	Num. Partitions κ	Top-1 Acc (%)
S-GaP	90%	uniform	1	75.9
S-GaP	90%	uniform	4	76.3

Table 7: The effect of different number of partitions for Transformer models on WMT-14 En-De.

Method	Sparsity Ratio	Distribution	Num. Partitions κ	SacreBLEU
S-GaP	90%	uniform	1	26.8
S-GaP	90%	uniform	3	27.7
S-GaP	90%	uniform	6	27.1

5 Theoretical Justification

We now provide the convergence guarantee for the cyclic-partitioned *S-GaP* algorithm. We let $F(\Theta) = \mathbb{E}_{x \sim D} f(x; \Theta)$ be the loss function of the deep learning task where D is the data distribution. In addition, we let m_q be the mask at the start of the q -th round, Θ_q be the learned model weights after $q - 1$ rounds, and $\Theta_q^{(i)}$, $i = 1, \dots, \kappa$ be the learned weights in the q -th round after the i -th partition is grown and trained for T epochs. Proposition 1 shows that *S-GaP* will converge to a neighborhood around the stationary solution at rate $\mathcal{O}(1/\sqrt{Q})$ when learning rate is set properly. Due to the space limitation, we put its proof in Appendix.

Proposition 1 (*S-GaP* CONVERGENCE). *Suppose the loss function $F(\Theta)$ is partition-wise L -smooth, the sampled stochastic gradient is unbiased and has bounded variance, and the relative error introduced by each mask is bounded by $\delta^2 \in [0, 1]$, i.e., $\|\Theta_q - \Theta_q \odot m_q\|^2 \leq \delta^2 \|\Theta_q\|^2$. If learning rate $\gamma = 1/(4\kappa LT\sqrt{Q})$, the sparse models generated by the cyclic-partitioned sequential *GaP* method after Q rounds will converge as follows:*

$$\frac{1}{Q} \sum_{q=1}^Q \mathbb{E} \|\nabla F(\Theta_q \odot m_q)\|^2 = \mathcal{O}\left(\frac{G}{\sqrt{Q}} + \frac{\delta^2}{Q} \sum_{q=1}^Q \sum_{i=1}^{\kappa} \mathbb{E} \|\Theta_q^{(i)}\|^2\right) \quad (1)$$

where G is a constant related to the gradient noise and the initialized model weights.

We make several remarks for Proposition 1 as follows.

Remark 1. *If there is no pruning in the training process, then it holds that $\delta^2 = 0$. Substituting it into (1), we find that *S-GaP* will converge exactly to a stationary solution, i.e., $\mathbb{E} \|\nabla F(\Theta_Q)\|^2 \rightarrow 0$ as Q increases to infinity. This implies *S-GaP* is also an effective algorithm even for dense training.*

Remark 2. *When a sparse mask is utilized, it holds that $\delta^2 \neq 0$. In this scenario, the mask-induced error will inevitably influence the accuracy of the trained model. A smaller mask-induced error will lead to a more accurate model that *S-GaP* can converge to.*

Remark 3. *In our proofs, we find that cycling through all partitions so that all weights can be trained per round is critical to guarantee the convergence of *S-GaP*. Note that previous work update weights either greedily (e.g., *RigL* [16]) or randomly (e.g., *SET* [14] and *DSR* [15]). It may take numerous training steps for these algorithms to have each weight explored and updated. This may explain why *S-GaP* achieves better accuracy than *RigL*, *SET*, and *DSR* (see Table 2). This intuition is consistent with [25, 26] which theoretically establish that sampling data cyclically converges faster than uniformly randomly in SGD training.*

Limitation. Our analysis in Proposition 1 cannot be directly extended to cover *P-GaP* since the analysis is built on the partition-wise cyclic updating structure of *S-GaP*. We will leave the analysis for *P-GaP* as a future work.

6 Related Works

In this section, we summarize the related works and explain the differences between their work and ours.

Pruning from pre-trained dense models: Among various pruning algorithms, one-shot pruning [27] zeros out a given percentage of the trained weights with the smallest magnitude. Based on the magnitude-based one-shot pruning, [28] proposes an iterative pruning method that progressively prune models to the target pruning ratio. However, those methods suffer from significant accuracy drop and relatively long training time. Besides magnitude-based pruning, other approaches [4, 29, 30] adapt mathematics-oriented regularization-based algorithms to generate sparsity. Later works [31, 19, 32, 33] utilizes dynamic regularization penalty such as Alternating Direction Methods of Multipliers (ADMM) [34, 35] to solve the pruning problem as an optimization problem and maintaining high accuracy. Other works such as DMCP [36], MetaPruning [37] use complicated rules to generate the sparsity distribution in the channel level. Since pre-training a dense model from which to select critical weights consumes large memory space, our work differs substantially from them such that we do not rely on a pre-trained dense model.

Pruning at an early stage: To reduce the theoretical training FLOPs, a new trend of exploring sparsity at an early stage [10, 11, 38, 39, 40] has emerged to embrace the promising sparse training paradigm. SNIP [10] finds the sparse masks based on the saliency score of each weight that is obtained after training the dense model for only a few iterations. GraSP [11] prunes weights based on preserving the gradient flow in the model. EarlyBird [12] conducts a retraining process after searching sub-network topology for a few epochs. PruneTrain [41] integrates structured pruning in the pretraining process. However, pruning at an early stage fails to achieve acceptable accuracy on ImageNet [42]. We recognize the underlying reason is that the single-shot pruning criterion is based on the information from a few mini-batch of training samples, which cannot accurately represent the rich features of large-scale dataset. The proposed GaP methods repeatedly update the sparse masks and hence overcome their drawbacks.

Sparse mask exploration: To satisfy the condition of low computation cost as well as low memory footprint, DeepR [13] firstly proposes to train a sparse network at initialization, and dynamically adjust the sparse topology by pruning the weights that flip the sign and randomly growing new weights during training. However, DeepR is primarily demonstrated with sparsification of fully-connected layers and applied to relatively small and shallow networks. Sparse Evolutionary Training (SET) [14] uses layer-wise magnitude-based pruning and random growth at the end of each training epoch. DSR [15] designs a dynamic reparameterization method that allows weights to be re-distributed across layers by dynamically adjusting the global pruning threshold. SNFS [43] develops sparse momentum to identify the importance of weights. RigL [16] proposes to use magnitude-based pruning and gradient-flow-based growth that update sparse model topology during training. All of the mentioned works update the sparse masks based on heuristics and there is little or no training at the mask update stage. Our work differs from them in that the mask updating rule of the GaP methods is more optimized by training a subset of layers into dense and then pruned.

7 Conclusions

Sparsity based model compression is gaining traction in research and industry to reduce the memory footprint and inference runtime. However, conventional compression approaches result to noticeable accuracy loss during the pruning process. In this paper, we propose a scheduled grow-and-prune (GaP) methodology to obtain sparse models. It divides a model into several partitions, grows and prunes each partition sequentially or in parallel. The experimental results show that this method preserves the model quality far better than previous work. In all four experimented tasks, the GaP method matches or even beats the dense solution at 80% sparsity. In addition, the GaP method does not require a pre-trained dense model and can continuously searching sparsity masks with new data, showing its flexibility and practical potential.

References

- [1] NVIDIA. NVIDIA A100 tensor core GPU architecture. Technical report, 2020.
- [2] Yiwen Guo, Anbang Yao, and Yurong Chen. Dynamic network surgery for efficient DNNs. In *Advances in Neural Information Processing Systems (NeurIPS)*, pages 1379–1387, 2016.
- [3] Ruichi Yu, Ang Li, Chun-Fu Chen, Jui-Hsin Lai, Vlad I Morariu, Xintong Han, Mingfei Gao, Ching-Yung Lin, and Larry S Davis. NISP: Pruning networks using neuron importance score propagation. In *Proceedings of the IEEE Conference on Computer Vision and Pattern Recognition (CVPR)*, pages 9194–9203, 2018.
- [4] Wei Wen, Chunpeng Wu, Yandan Wang, Yiran Chen, and Hai Li. Learning structured sparsity in deep neural networks. In *Advances in Neural Information Processing Systems (NeurIPS)*, pages 2074–2082, 2016.
- [5] Zhuang Liu, Mingjie Sun, Tinghui Zhou, Gao Huang, and Trevor Darrell. Rethinking the value of network pruning. In *International Conference on Learning Representations (ICLR)*, 2019.
- [6] Barret Zoph and Quoc V Le. Neural architecture search with reinforcement learning. In *International Conference on Learning Representations (ICLR)*, 2017.
- [7] Gabriel Bender, Pieter-Jan Kindermans, Barret Zoph, Vijay Vasudevan, and Quoc Le. Understanding and simplifying one-shot architecture search. In *International Conference on Machine Learning (ICML)*, pages 550–559. PMLR, 2018.
- [8] Hieu Pham, Melody Guan, Barret Zoph, Quoc Le, and Jeff Dean. Efficient neural architecture search via parameters sharing. In *International Conference on Machine Learning (ICML)*, pages 4095–4104. PMLR, 2018.
- [9] Esteban Real, Alok Aggarwal, Yanping Huang, and Quoc V Le. Regularized evolution for image classifier architecture search. In *Proceedings of the AAAI Conference on Artificial Intelligence*, volume 33, pages 4780–4789, 2019.
- [10] Namhoon Lee, Thalaiyasingam Ajanthan, and Philip Torr. SNIP: Single-shot network pruning based on connection sensitivity. In *International Conference on Learning Representations (ICLR)*, 2019.
- [11] Chaoqi Wang, Guodong Zhang, and Roger Grosse. Picking winning tickets before training by preserving gradient flow. In *International Conference on Learning Representations (ICLR)*, 2020.
- [12] Haoran You, Chaojian Li, Pengfei Xu, Yonggan Fu, Yue Wang, Xiaohan Chen, Yingyan Lin, Zhangyang Wang, and Richard G. Baraniuk. Drawing early-bird tickets: Toward more efficient training of deep networks. In *International Conference on Learning Representations (ICLR)*, 2020.
- [13] Guillaume Bellec, David Kappel, Wolfgang Maass, and Robert Legenstein. Deep rewiring: Training very sparse deep networks. In *International Conference on Learning Representations (ICLR)*, 2018.
- [14] Decebal Constantin Mocanu, Elena Mocanu, Peter Stone, Phuong H Nguyen, Madeleine Gibescu, and Antonio Liotta. Scalable training of artificial neural networks with adaptive sparse connectivity inspired by network science. *Nature Communications*, 9(1):1–12, 2018.
- [15] Hesham Mostafa and Xin Wang. Parameter efficient training of deep convolutional neural networks by dynamic sparse reparameterization. In *International Conference on Machine Learning (ICML)*, pages 4646–4655. PMLR, 2019.
- [16] Utku Evci, Trevor Gale, Jacob Menick, Pablo Samuel Castro, and Erich Elsen. Rigging the lottery: Making all tickets winners. In *International Conference on Machine Learning (ICML)*, pages 2943–2952. PMLR, 2020.
- [17] NVIDIA. <https://github.com/NVIDIA/DeepLearningExamples>, 2020.
- [18] Xu Yan. Pointnet/pointnet++ pytorch. https://github.com/yanx27/Pointnet_Pointnet2_pytorch, 2019.
- [19] Ao Ren, Tianyun Zhang, Shaokai Ye, Jiayu Li, Wenyao Xu, Xuehai Qian, Xue Lin, and Yanzhi Wang. ADMM-NN: An algorithm-hardware co-design framework of DNNs using alternating direction methods of multipliers. In *Proceedings of the Twenty-Fourth International Conference on Architectural Support for Programming Languages and Operating Systems*, pages 925–938. ACM, 2019.
- [20] Tao Lin, Sebastian U. Stich, Luis Barba, Daniil Dmitriev, and Martin Jaggi. Dynamic model pruning with feedback. In *International Conference on Learning Representations*, 2020.
- [21] Charles R Qi, Li Yi, Hao Su, and Leonidas J Guibas. Pointnet++: Deep hierarchical feature learning on point sets in a metric space. *arXiv preprint arXiv:1706.02413*, 2017.
- [22] Li Yi, Vladimir G Kim, Duygu Ceylan, I-Chao Shen, Mengyan Yan, Hao Su, Cewu Lu, Qixing Huang, Alla Sheffer, and Leonidas Guibas. A scalable active framework for region annotation in 3D shape collections. *ACM Transactions on Graphics (ToG)*, 35(6):1–12, 2016.

[23] Ashish Vaswani, Noam Shazeer, Niki Parmar, Jakob Uszkoreit, Llion Jones, Aidan N Gomez, Łukasz Kaiser, and Illia Polosukhin. Attention is all you need. In *Advances in Neural Information Processing Systems (NeurIPS)*, pages 5998–6008, 2017.

[24] Matt Post. A call for clarity in reporting BLEU scores. In *Proceedings of the Third Conference on Machine Translation: Research Papers*, pages 186–191, Belgium, Brussels, October 2018. Association for Computational Linguistics.

[25] Mert Gürbüzbalaban, Asu Ozdaglar, and Pablo A Parrilo. Why random reshuffling beats stochastic gradient descent. *Mathematical Programming*, pages 1–36, 2019.

[26] Bicheng Ying, Kun Yuan, Stefan Vlaski, and Ali H Sayed. Stochastic learning under random reshuffling with constant step-sizes. *IEEE Transactions on Signal Processing*, 67(2):474–489, 2018.

[27] Yann LeCun, John S Denker, and Sara A Solla. Optimal brain damage. In *Advances in neural information processing systems*, pages 598–605, 1990.

[28] Song Han, Huizi Mao, and William J. Dally. Deep compression: Compressing deep neural networks with pruning, trained quantization and Huffman coding. In *International Conference on Learning Representations (ICLR)*, 2016.

[29] Yihui He, Xiangyu Zhang, and Jian Sun. Channel pruning for accelerating very deep neural networks. In *Proceedings of the IEEE International Conference on Computer Vision (ICCV)*, pages 1389–1397, 2017.

[30] Christos Louizos, Max Welling, and Diederik P Kingma. Learning sparse neural networks through L_0 regularization. In *International Conference on Learning Representations (ICLR)*, 2018.

[31] Tianyun Zhang, Shaokai Ye, Kaiqi Zhang, Jian Tang, Wujie Wen, Makan Fardad, and Yanzhi Wang. A systematic DNN weight pruning framework using alternating direction method of multipliers. In *Proceedings of the European Conference on Computer Vision (ECCV)*, pages 184–199, 2018.

[32] Xiaolong Ma, Fu-Ming Guo, Wei Niu, Xue Lin, Jian Tang, Kaisheng Ma, Bin Ren, and Yanzhi Wang. Pconv: The missing but desirable sparsity in DNN weight pruning for real-time execution on mobile devices. In *Proceedings of the AAAI Conference on Artificial Intelligence*, volume 34, pages 5117–5124, 2020.

[33] Xiaolong Ma, Wei Niu, Tianyun Zhang, Sijia Liu, Sheng Lin, Hongjia Li, Wujie Wen, Xiang Chen, Jian Tang, Kaisheng Ma, et al. An image enhancing pattern-based sparsity for real-time inference on mobile devices. In *Proceedings of the European conference on computer vision (ECCV)*, pages 629–645. Springer, 2020.

[34] Stephen Boyd, Neal Parikh, Eric Chu, Borja Peleato, and Jonathan Eckstein. Distributed optimization and statistical learning via the alternating direction method of multipliers. *Foundations and Trends® in Machine Learning*, 3(1):1–122, 2011.

[35] Hua Ouyang, Niao He, Long Tran, and Alexander Gray. Stochastic alternating direction method of multipliers. In *International Conference on Machine Learning*, pages 80–88. PMLR, 2013.

[36] Shaopeng Guo, Yujie Wang, Quanquan Li, and Junjie Yan. DMCP: Differentiable Markov channel pruning for neural networks. In *Proceedings of the IEEE/CVF Conference on Computer Vision and Pattern Recognition*, pages 1539–1547, 2020.

[37] Zechun Liu, Haoyuan Mu, Xiangyu Zhang, Zichao Guo, Xin Yang, Kwang-Ting Cheng, and Jian Sun. MetaPruning: Meta learning for automatic neural network channel pruning. In *Proceedings of the IEEE/CVF International Conference on Computer Vision*, pages 3296–3305, 2019.

[38] Hidenori Tanaka, Daniel Kunin, Daniel L Yamins, and Surya Ganguli. Pruning neural networks without any data by iteratively conserving synaptic flow. *Advances in Neural Information Processing Systems (NeurIPS)*, 33, 2020.

[39] Paul Wimmer, Jens Mehnert, and Alexandru Condurache. Freezenet: Full performance by reduced storage costs. In *Proceedings of the Asian Conference on Computer Vision (ACCV)*, 2020.

[40] Joost van Amersfoort, Milad Alizadeh, Sebastian Farquhar, Nicholas Lane, and Yarin Gal. Single shot structured pruning before training. *arXiv preprint arXiv:2007.00389*, 2020.

[41] Sangkug Lym, Esha Choukse, Siavash Zangeneh, Wei Wen, Sujay Sanghavi, and Mattan Erez. PruneTrain: fast neural network training by dynamic sparse model reconfiguration. In *Proceedings of the International Conference for High Performance Computing, Networking, Storage and Analysis*, pages 1–13, 2019.

[42] Jia Deng, Wei Dong, Richard Socher, Li-Jia Li, Kai Li, and Li Fei-Fei. ImageNet: A large-scale hierarchical image database. In *Proceedings of the IEEE Conference on Computer Vision and Pattern Recognition (CVPR)*, pages 248–255, 2009.

[43] Tim Dettmers and Luke Zettlemoyer. Sparse networks from scratch: Faster training without losing performance. *NeurIPS*, 2019.

A More ablation study

A.1 Partition the model in a random manner

In the main context, each partition of the model consists of contiguous layers and they are cyclically grown and pruned. We also explore a random partition strategy for each step in the *S*-GaP for sparse ResNet-50 models. Unlike the cyclic partition, a random partition chooses a uniformly random subset of layers to grow in each step of the GaP process. From Table 8, we observe that the random partition is slightly worse than the cyclic partition but still better than all previous existing solutions.

Table 8: Different partition strategies for ResNet-50 models on ImageNet.

Method	Sparsity Ratio	Distribution	Num. Partitions	Partition strategy	Top-1 Acc (%)
S -GaP	90%	non-uniform	4	Cyclic	77.9
S -GaP	90%	non-uniform	4	Random	77.8

A.2 Generalization to other sparse granularity

We use unstructured sparsity throughout the paper. In this section, we demonstrate that the GaP method is also applicable to other coarse-grained sparse granularity such as block-wise sparsity. The unit for the block-wise sparsity in this experiment is 1×8 , i.e., if the weight matrix is viewed as many 1×8 blocks, then the sparsity ratio of the matrix is defined as the ratio of *all-zero* blocks. It is often believed that the accuracy would be impacted severely when the block size is 8 or greater. Table 9 compares the SacreBleu scores of the sparse Transformer models obtained by applying the 3-partition cyclic *S*-GaP and the prune-from-dense methods. It is observed that the GaP method improves over the prune-from-dense method significantly (27.21 vs. 26.21). This further validates the benefits of mask updating strategy brought by the GaP method.

Table 9: Different sparsifying methods for the Transformer models with structured sparsity on WMT-14 En-De.

Method	Sparsity Ratio	sparse granularity	Num. Partitions κ	BLEU
prune-from-dense	80%	block 1×8	-	26.1
S -GaP	80%	block 1×8	3	27.2

A.3 Pruning the fully connected layer in the ResNet-50 model

In the main context, the last fully connected (FC) layer of the ResNet-50 model is kept dense in the uniform sparsity distribution since it contributes to less than 1% of the FLOPs. In Table 10, we perform additional experiments to supplement Table 2 by pruning the last FC layer using the *S*-GaP method and comparing them with [16]. The results in Table 10 and Table 2 indicate that the accuracy of the ResNet-50 models with sparse and dense FC layers are similar, and both of them outperform the state-of-the-art results in [16]. Please note that models with the non-uniform sparsifying distribution in Table 2 already have the last FC layer pruned, thus the experiment setup is the same as the ones in [16].

Table 10: Results of sparse ResNet-50 models on ImageNet.

Method	Distribution	Sparsity ratio: 80%		Sparsity ratio: 90%	
		Top-1 Acc (%)	FLOPS ($\times 10^9$)	Top-1 Acc (%)	FLOPS ($\times 10^9$)
RigL [16]	uniform	74.6	1.7	72.0	0.8
RigL ₅ [16]	uniform	76.6	1.7	75.7	0.8
S -GaP (dense FC)	uniform	77.9	1.7	76.3	0.8
S -GaP (sparse FC)	uniform	77.8	1.7	76.4	0.8

B Some more descriptions on the parallel GaP method

In this section, we provide a graphical description in Figure 3 on the parallel GaP method that is similar to Figure 1 for the sequential GaP method. Note that in Figure 3, when the four dense partitions are combined in the central node, no training is required. The fully dense model is pruned and then redistributed to four nodes for training.

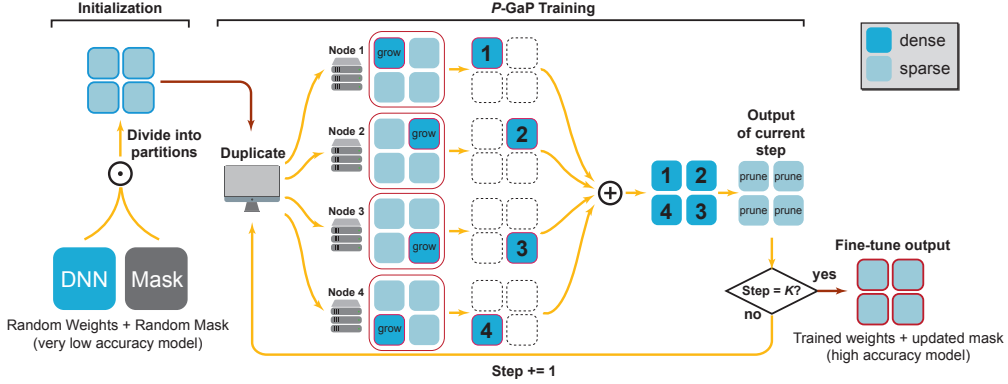


Figure 3: Overview of the parallel GaP (P -GaP) training method. We assume 4 training nodes are used for the 4 partitions, which are grown in parallel for T epochs. At the end of each step, the dense parts in the nodes are combined, followed by a pruning back to a sparse model. After K steps, the model is fine-tuned.

C Proof of Proposition 1

C.1 Problem formulation

Training deep neural networks can be formulated into minimizing the following problem:

$$\min_{\Theta \in \mathbb{R}^d} F(\Theta) = \mathbb{E}_{x \sim D}[f(x; \Theta)] \quad (2)$$

where $\Theta \in \mathbb{R}^d$ is the model parameter to be learned, and $f(x; \Theta)$ is a smooth non-convex cost function in terms of Θ . The random variable x denotes the data samples that follow the distribution D . $\mathbb{E}_{x \sim D}[\cdot]$ denotes the expectation over the random variable x .

C.2 Notation

We first clarify the notions used in the convergence analysis. To characterize how GaP updates model parameters in a partition-wise manner, we introduce matrices $U_i \in \mathbb{R}^{d \times d_i}$, $i = 1, \dots, \kappa$, for which the identity matrix $I_d \in \mathbb{R}^{d \times d}$ can be represented as

$$I_d = (U_1, U_2, \dots, U_\kappa). \quad (3)$$

- $\Theta^{S_i} = U_i^T \Theta \in \mathbb{R}^{d_i}$ is the model parameter at the i -th partition (i.e., partition S_i).
- $m^{S_i} \in \mathbb{R}^{d_i}$ is the mask for the i -th partition.
- $\nabla f(x; \Theta) \in \mathbb{R}^d$ and $\nabla F(\Theta) \in \mathbb{R}^d$ are the complete stochastic and accurate gradients in terms of Θ , respectively.
- $\nabla_i f(x; \Theta) = U_i^T \nabla f(x; \Theta) \in \mathbb{R}^{d_i}$ is the stochastic gradient for the i -th partition
- $\nabla_i F(\Theta) = U_i^T \nabla F(\Theta) \in \mathbb{R}^{d_i}$ is the gradient for the i -th partition.
- $\Theta_{q,t}^{(i)} \in \mathbb{R}^d$ denotes the complete model parameter in which its i -th partition (i.e., $[\Theta_{q,t}^{(i)}]^{S_i} \in \mathbb{R}^{d_i}$) is newly updated at the q -th round and t -th inner iteration while the other partitions remain unchanged.
- $m_q^{(i)} \in \mathbb{R}^d$ is a complete mask vector for the i -th partition in the q -th round.
- $x_{q,t}^{(i)}$ is the data sampled at q -th round and t -th inner iteration to update the i -th partition.

C.3 Algorithm reformulation

In this subsection we reformulate the sequential GaP (*S*-Gap) in Algorithm 1 in a way that can present the convergence analysis more easily. With the notations in Sec. C.2, the *S*-Gap Algorithm 1 can be reformulated as

Algorithm 3: *S*-GaP Algorithm (A math-friendly version)

Initialize $\Theta_{1,0}^{(1)}$ and $m_1^{(0)}$ randomly. Initialize pruning ratio r .

for round $q = 1, 2, \dots, Q$ **do**

for partition $i = 1, 2, \dots, \kappa$ **do**
 | Generate a mask $m_q^{(i)} = \text{GaPMask}(\Theta_{q,0}^{(i)}, m_q^{(i-1)}, r)$;
 | **for** $t = 1, \dots, T$ **do**
 | | Update $\Theta_{q,t}^{(i)} = \Theta_{q,t-1}^{(i)} - \gamma U_i \nabla_i f(x_{q,t-1}^{(i)}; \Theta_{q,t-1}^{(i)} \odot m_q^{(i)})$
 | | Update $\Theta_{q,0}^{(i+1)} = \Theta_{q,T}^{(i)}$
 | | Update $\Theta_{q+1,0}^{(1)} = \Theta_{q,T}^{(\kappa+1)}$ and $m_{q+1}^{(0)} = m_q^{(\kappa)}$;

Output: $\Theta_{Q,T}^{(\kappa)} \odot m_Q^{(\kappa)}$.

In $\text{GaPMask}(\Theta_{q,0}^{(i)}, m_q^{(i-1)}, r)$, the partition of $[m_q^{(i)}]^{S_i}$ is updated as:

Prune $(i-1)$ -th partition: update $[m_q^{(i)}]^{S_{i-1}} \leftarrow \text{ArgPruneTo}([\Theta_{q,t}^{(i)}]^{S_{i-1}}, r)$ for pruning ratio r

Grow i -th partition: Let $[m_q^{(i)}]^{S_i} = \mathbb{1}_{d_i} \in \mathbb{R}^{d_i}$

Other j -th partition: $[m_q^{(i)}]^{S_j} = [m_q^{(i-1)}]^{S_j}$ (for all $j \neq i$ and $j \neq i-1$)

and $m_q^{(i)} = [m_q^{(i)}]^{S_1 \cup S_2 \cup \dots \cup S_\kappa}$.

C.4 Assumptions

We now introduce several assumptions on the cost function and the gradient noise, which are standard in the literature.

Assumption 1 (SMOOTHNESS). *We assume the cost function $F(\Theta)$ is partition-wise L -smooth, i.e.,*

$$\|\nabla_i F(\Theta + U_i h_i) - \nabla_i F(\Theta)\| \leq L\|h_i\|, \quad \forall h_i \in \mathbb{R}^{d_i}. \quad (4)$$

The above assumption implies that

$$\|\nabla F(\Theta) - \nabla F(\Phi)\| \leq L\|\Theta - \Phi\|, \quad \forall \Theta, \Phi \in \mathbb{R}^d, \quad (5)$$

or equivalently,

$$F(\Theta) - F(\Phi) \leq \langle \nabla F(\Phi), \Theta - \Phi \rangle + \frac{L}{2}\|\Theta - \Phi\|^2, \quad \forall \Theta, \Phi \in \mathbb{R}^d, \quad (6)$$

Assumption 2 (GRADIENT NOISE). *We assume for any k, t , and i that*

$$\mathbb{E}[\nabla_i f(x_{q,t}^{(i)}; \Theta)] = \nabla_i F(\Theta), \quad (7)$$

$$\mathbb{E}[\|\nabla_i f(x_{q,t}^{(i)}; \Theta) - \nabla_i F(\Theta)\|^2] \leq \sigma^2, \quad (8)$$

where $\sigma > 0$ is a constant. Moreover, we assume the data sample $x_{q,t}^{(i)}$ is independent of each other for any k, t , and i .

This assumption implies that the stochastic partition-gradient is unbiased and has bounded variance.

Assumption 3 (MASK-INCURRED ERROR). *It is assumed that*

$$\|\Theta_{q,t-1}^{(i)} \odot m_q^{(i)} - \Theta_{q,t-1}^{(i)}\|^2 \leq \delta^2 \|\Theta_{q,t-1}^{(i)}\|^2 \quad \text{where } \delta \in (0, 1). \quad (9)$$

Note that $[m_q^{(i)}]^{S_i} = \mathbb{1}_{d_i}$, and only the i -th partition in $\Theta_{q,t}^{(i)}$ is got updated during iterations $(q, 1), \dots, (q, T)$, we have

$$\|\Theta_{q,t-1}^{(i)} \odot m_q^{(i)} - \Theta_{q,t-1}^{(i)}\|^2 = \|\Theta_{q,0}^{(i)} \odot m_q^{(i)} - \Theta_{q,0}^{(i)}\|^2 \leq \delta^2 \|\Theta_{q,0}^{(i)}\|^2. \quad (10)$$

C.5 Convergence analysis

Now we are ready to establish the convergence property of S -GaP in Algorithm 3. The arguments to establish the convergence are strait-forward:

- First, we need to establish the function value $\mathbb{E}[F(\Theta_{q,t-1}^{(i)})]$ will *decrease* to $\mathbb{E}[F(\Theta_{q,t}^{(i)})]$, up to an error term caused by the gradient noise and mask pruning, after each inner-iteration t when updating the i -th partition (See Lemma 1).
- Based on the above fact, we next prove $\mathbb{E}[F(\Theta_{q,0}^{(i)})]$ will *decrease* to $\mathbb{E}[F(\Theta_{q,0}^{(i+1)})]$ when T -steps training of the i -th partition is completed (See Lemma 2).
- Finally, with the second fact, we show that $\mathbb{E}[F(\Theta_{q,0}^{(1)})]$ will *decrease* to $\mathbb{E}[F(\Theta_{q+1,0}^{(1)})]$ after the k -th outer round (See Lemmas 3 and 4). Since the function value decreases for each round k , we can prove that S -GaP will converge to a stationary solution after sufficiently large Q rounds (See Theorem 1).

Next we present the detail analysis.

Lemma 1 (DESCENT LEMMA AFTER EACH INNER-ITERATION). *Under Assumptions 1-3, it holds for each k , i , and t that*

$$\mathbb{E}[F(\Theta_{q,t}^{(i)})] \leq \mathbb{E}[F(\Theta_{q,t-1}^{(i)})] - \frac{\gamma}{3} \mathbb{E}\|\nabla_i F(\Theta_{q,t-1}^{(i)})\|^2 + \frac{\gamma^2 L \sigma^2}{2} + \frac{2\gamma L^2 \delta^2}{3} \mathbb{E}\|\Theta_{q,0}^{(i)}\|^2. \quad (11)$$

Remark 4. *It is observed in Lemma 1 that the function value will decrease by $\frac{\gamma}{3} \mathbb{E}\|\nabla_i F(\Theta_{q,t-1}^{(i)})\|^2$ for each inner-iteration t . But such decrement suffers from two error terms: one is caused by stochastic gradient noise, and the other is by inexact pruning.*

Proof. Since $F(\Theta)$ is L -smooth (see Assumption 1), it holds that

$$\begin{aligned} F(\Theta_{q,t}^{(i)}) &\leq F(\Theta_{q,t-1}^{(i)}) + \langle \nabla F(\Theta_{q,t-1}^{(i)}), \Theta_{q,t}^{(i)} - \Theta_{q,t-1}^{(i)} \rangle + \frac{L}{2} \|\Theta_{q,t}^{(i)} - \Theta_{q,t-1}^{(i)}\|^2 \\ &= F(\Theta_{q,t-1}^{(i)}) - \gamma \langle \nabla_i F(\Theta_{q,t-1}^{(i)}), \nabla_i f(x_{q,t-1}^{(i)}; \Theta_{q,t-1}^{(i)} \odot m_q^{(i)}) \rangle \\ &\quad + \frac{\gamma^2 L}{2} \|\nabla_i f(x_{q,t-1}^{(i)}; \Theta_{q,t-1}^{(i)} \odot m_q^{(i)})\|^2 \end{aligned} \quad (12)$$

With Assumption 2, it is easy to verify that

$$\begin{aligned} &\mathbb{E}\langle \nabla_i F(\Theta_{q,t-1}^{(i)}), \nabla_i f(x_{q,t-1}^{(i)}; \Theta_{q,t-1}^{(i)} \odot m_q^{(i)}) \rangle \\ &= \mathbb{E}_{\Theta_{q,t-1}^{(i)}} \left\{ \mathbb{E}[\langle \nabla_i F(\Theta_{q,t-1}^{(i)}), \nabla_i f(x_{q,t-1}^{(i)}; \Theta_{q,t-1}^{(i)} \odot m_q^{(i)}) \rangle | \Theta_{q,t-1}^{(i)}] \right\} \\ &\stackrel{(7)}{=} \mathbb{E}\langle \nabla_i F(\Theta_{q,t-1}^{(i)}), \nabla_i F(\Theta_{q,t-1}^{(i)} \odot m_q^{(i)}) \rangle. \end{aligned} \quad (13)$$

Using a similar way, we can prove, with (8), that

$$\mathbb{E}\|\nabla_i f(x_{q,t-1}^{(i)}; \Theta_{q,t-1}^{(i)} \odot m_q^{(i)})\|^2 \leq \mathbb{E}\|\nabla_i F(\Theta_{q,t-1}^{(i)} \odot m_q^{(i)})\|^2 + \sigma^2 \quad (14)$$

By taking the expectation over (12) and substituting (13) and (14) into (12), we achieve

$$\begin{aligned} \mathbb{E}[F(\Theta_{q,t}^{(i)})] &\leq \mathbb{E}[F(\Theta_{q,t-1}^{(i)})] - \gamma \mathbb{E}\langle \nabla_i F(\Theta_{q,t-1}^{(i)}), \nabla_i F(\Theta_{q,t-1}^{(i)} \odot m_q^{(i)}) \rangle \\ &\quad + \frac{\gamma^2 L}{2} \mathbb{E}\|\nabla_i F(\Theta_{q,t-1}^{(i)} \odot m_q^{(i)})\|^2 + \frac{\gamma^2 L \sigma^2}{2} \\ &= \mathbb{E}[F(\Theta_{q,t-1}^{(i)})] - \gamma \mathbb{E}\|\nabla_i F(\Theta_{q,t-1}^{(i)})\|^2 + \frac{\gamma^2 L}{2} \mathbb{E}\|\nabla_i F(\Theta_{q,t-1}^{(i)} \odot m_q^{(i)})\|^2 + \frac{\gamma^2 L \sigma^2}{2} \end{aligned}$$

$$-\gamma \mathbb{E} \langle \nabla_i F(\Theta_{q,t-1}^{(i)}), \nabla_i F(\Theta_{q,t-1}^{(i)} \odot m_q^{(i)}) - \nabla_i F(\Theta_{q,t-1}^{(i)}) \rangle. \quad (15)$$

Note that

$$\begin{aligned} & \mathbb{E} \|\nabla_i F(\Theta_{q,t-1}^{(i)} \odot m_q^{(i)})\|^2 \\ & \leq 2\mathbb{E} \|\nabla_i F(\Theta_{q,t-1}^{(i)})\|^2 + 2\mathbb{E} \|\nabla_i F(\Theta_{q,t-1}^{(i)}) - \nabla_i F(\Theta_{q,t-1}^{(i)} \odot m_q^{(i)})\|^2 \\ & \leq 2\mathbb{E} \|\nabla_i F(\Theta_{q,t-1}^{(i)})\|^2 + 2\mathbb{E} \|\nabla F(\Theta_{q,t-1}^{(i)}) - \nabla F(\Theta_{q,t-1}^{(i)} \odot m_q^{(i)})\|^2 \\ & \stackrel{(5)}{\leq} 2\mathbb{E} \|\nabla_i F(\Theta_{q,t-1}^{(i)})\|^2 + 2L^2 \mathbb{E} \|\Theta_{q,t-1}^{(i)} \odot m_q^{(i)} - \Theta_{q,t-1}^{(i)}\|^2 \\ & \stackrel{(10)}{\leq} 2\mathbb{E} \|\nabla_i F(\Theta_{q,t-1}^{(i)})\|^2 + 2L^2 \delta^2 \mathbb{E} \|\Theta_{q,0}^{(i)}\|^2 \end{aligned} \quad (16)$$

and, similarly,

$$\begin{aligned} & -\mathbb{E} \langle \nabla_i F(\Theta_{q,t-1}^{(i)}), \nabla_i F(\Theta_{q,t-1}^{(i)} \odot m_q^{(i)}) - \nabla_i F(\Theta_{q,t-1}^{(i)}) \rangle \\ & \leq \frac{1}{2} \mathbb{E} \|\nabla_i F(\Theta_{q,t-1}^{(i)})\|^2 + \frac{1}{2} \mathbb{E} \|\nabla_i F(\Theta_{q,t-1}^{(i)} \odot m_q^{(i)}) - \nabla_i F(\Theta_{q,t-1}^{(i)})\|^2 \\ & \leq \frac{1}{2} \mathbb{E} \|\nabla_i F(\Theta_{q,t-1}^{(i)})\|^2 + \frac{L^2 \delta^2}{2} \mathbb{E} \|\Theta_{q,0}^{(i)}\|^2 \end{aligned} \quad (17)$$

Substituting (16) and (17) into (15), and by setting $\gamma \leq 1/(6L)$, we have

$$\begin{aligned} \mathbb{E}[F(\Theta_{q,t}^{(i)})] & \leq \mathbb{E}[F(\Theta_{q,t-1}^{(i)})] - \frac{\gamma(1-2\gamma L)}{2} \mathbb{E} \|\nabla_i F(\Theta_{q,t-1}^{(i)})\|^2 + \frac{\gamma^2 L \sigma^2}{2} \\ & \quad + \frac{\gamma L^2 \delta^2 (1+2\gamma L)}{2} \mathbb{E} \|\Theta_{q,0}^{(i)}\|^2 \\ & \leq \mathbb{E}[F(\Theta_{q,t-1}^{(i)})] - \frac{\gamma}{3} \mathbb{E} \|\nabla_i F(\Theta_{q,t-1}^{(i)})\|^2 + \frac{\gamma^2 L \sigma^2}{2} + \frac{2\gamma L^2 \delta^2}{3} \mathbb{E} \|\Theta_{q,0}^{(i)}\|^2. \end{aligned} \quad (18)$$

□

Lemma 2 (DESCENT LEMMA AFTER EACH PARTITION UPDATE). *Under Assumptions 1-3, it holds for each k and i that*

$$\mathbb{E}[F(\Theta_{q,0}^{(i)})] \leq \mathbb{E}[F(\Theta_{q,0}^{(i+1)})] - \frac{\gamma}{3} \sum_{t=1}^T \mathbb{E} \|\nabla_i F(\Theta_{q,t-1}^{(i)})\|^2 + \frac{\gamma^2 L \sigma^2 T}{2} + \frac{2\gamma L^2 \delta^2 T}{3} \mathbb{E} \|\Theta_{q,0}^{(i)}\|^2 \quad (19)$$

Proof. Summing the inequality over (11) for $t = 1, \dots, T$, we achieve

$$\begin{aligned} \frac{\gamma}{3} \sum_{t=1}^T \mathbb{E} \|\nabla_i F(\Theta_{q,t-1}^{(i)})\|^2 & \leq \sum_{t=1}^T \mathbb{E} [F(\Theta_{q,t-1}^{(i)}) - F(\Theta_{q,t}^{(i)})] + \frac{\gamma^2 L \sigma^2 T}{2} + \frac{2\gamma L^2 \delta^2 T}{3} \mathbb{E} \|\Theta_{q,0}^{(i)}\|^2 \\ & = \mathbb{E} [F(\Theta_{q,0}^{(i)}) - F(\Theta_{q,T}^{(i)})] + \frac{\gamma^2 L \sigma^2 T}{2} + \frac{2\gamma L^2 \delta^2 T}{3} \mathbb{E} \|\Theta_{q,0}^{(i)}\|^2 \end{aligned} \quad (20)$$

which completes the proof. □

Lemma 3 (DESCENT LEMMA AFTER EACH ROUND). *Under Assumptions 1-3, it holds for each k that*

$$\begin{aligned} \mathbb{E}[F(\Theta_{q,0}^{(1)})] & \leq \mathbb{E}[F(\Theta_{q+1,0}^{(1)})] - \frac{\gamma}{3} \sum_{i=1}^{\kappa} \sum_{t=1}^T \mathbb{E} \|\nabla_i F(\Theta_{q,t-1}^{(i)})\|^2 \\ & \quad + \frac{\gamma^2 L \sigma^2 T \kappa}{2} + \frac{2\gamma L^2 \delta^2 T}{3} \sum_{i=1}^{\kappa} \mathbb{E} \|\Theta_{q,0}^{(i)}\|^2 \end{aligned} \quad (21)$$

Proof. Summing the inequality in (19) over $i = 1, \dots, \kappa$, we have

$$\sum_{i=1}^{\kappa} \sum_{t=1}^T \mathbb{E} \|\nabla_i F(\Theta_{q,t-1}^{(i)})\|^2 \leq \frac{3}{\gamma} \sum_{i=1}^{\kappa} \mathbb{E} [F(\Theta_{q,0}^{(i)}) - F(\Theta_{q,T}^{(i)})] + \frac{3\gamma L\sigma^2 T \kappa}{2} + 2L^2 \delta^2 T \sum_{i=1}^{\kappa} \mathbb{E} \|\Theta_{q,0}^{(i)}\|^2 \quad (22)$$

On the other hand, by the updating rule of $\Theta_{q,0}^{(i)}$, we have

$$\begin{aligned} \sum_{i=1}^{\kappa} \mathbb{E} [F(\Theta_{q,0}^{(i)}) - F(\Theta_{q,T}^{(i)})] &= \mathbb{E} [F(\Theta_{q,0}^{(\kappa)}) - F(\Theta_{q,T}^{(\kappa)})] + \sum_{i=1}^{\kappa-1} \mathbb{E} [F(\Theta_{q,0}^{(i)}) - F(\Theta_{q,T}^{(i)})] \\ &= \mathbb{E} [F(\Theta_{q,0}^{(\kappa)}) - F(\Theta_{q+1,0}^{(1)})] + \sum_{i=1}^{\kappa-1} \mathbb{E} [F(\Theta_{q,0}^{(i)}) - F(\Theta_{q,0}^{(i+1)})] \\ &= \mathbb{E} [F(\Theta_{q,0}^{(1)}) - F(\Theta_{q+1,0}^{(1)})]. \end{aligned} \quad (23)$$

Substituting (23) into (22), we achieve

$$\begin{aligned} &\sum_{i=1}^{\kappa} \sum_{t=1}^T \mathbb{E} \|\nabla_i F(\Theta_{q,t-1}^{(i)})\|^2 \\ &\leq \frac{3}{\gamma} \left(\mathbb{E} [F(\Theta_{q,0}^{(1)}) - F(\Theta_{q+1,0}^{(1)})] \right) + \frac{3\gamma L\sigma^2 T \kappa}{2} + 2L^2 \delta^2 T \sum_{i=1}^{\kappa} \mathbb{E} \|\Theta_{q,0}^{(i)}\|^2 \end{aligned} \quad (24)$$

which completes the proof. \square

To finish the convergence proof, we still need to establish the relation between the decrement $\sum_{i=1}^{\kappa} \sum_{t=1}^T \mathbb{E} \|\nabla_i F(\Theta_{q,t-1}^{(i)})\|^2$ and $\mathbb{E} \|\nabla F(\Theta_{q,0}^{(1)})\|^2$ so that

Lemma 4 (DESCENT LEMMA II AFTER EACH ROUND). *Under Assumptions 1-3, and learning rate $\gamma \leq \frac{1}{4\kappa L T}$, it holds for each k that*

$$\mathbb{E} [F(\Theta_{q,0}^{(1)})] \leq \mathbb{E} [F(\Theta_{q+1,0}^{(1)})] - \frac{\gamma T}{12} \mathbb{E} \|\nabla F(\Theta_{q,0}^{(1)})\|^2 + \frac{\gamma^2 L\sigma^2 T^2 \kappa}{6} + \frac{2\gamma L^2 \delta^2 T^2}{3} \sum_{i=1}^{\kappa} \mathbb{E} \|\Theta_{q,0}^{(i)}\|^2 \quad (25)$$

Proof. In the following we lower bound the term $\sum_{i=1}^{\kappa} \sum_{t=1}^T \mathbb{E} \|\nabla_i F(\Theta_{q,t-1}^{(i)})\|^2$ in (21). Recall Algorithm 3 that

$$\Theta_{q,0}^{(i+1)} = \Theta_{q,0}^{(i)} - \gamma U_i \sum_{t=1}^T \nabla_i f(x_{q,t-1}^{(i)}; \Theta_{q,t-1}^{(i)} \odot m_q^{(i)}), \quad (26)$$

$$\Theta_{q,t}^{(i)} = \Theta_{q,0}^{(i)} - \gamma U_i \sum_{s=1}^t \nabla_i f(x_{q,s-1}^{(i)}; \Theta_{q,s-1}^{(i)} \odot m_q^{(i)}). \quad (27)$$

With these relations, it holds for $i \geq 1$ and $t \geq 1$ that

$$\begin{aligned} &\mathbb{E} \|\Theta_{q,t}^{(i)} - \Theta_{q,0}^{(1)}\|^2 \\ &= \mathbb{E} \|\Theta_{q,t}^{(i)} - \Theta_{q,0}^{(i)} + \Theta_{q,0}^{(i)} - \Theta_{q,0}^{(i-1)} + \dots + \Theta_{q,0}^{(2)} - \Theta_{q,0}^{(1)}\|^2 \\ &\stackrel{(a)}{=} \mathbb{E} \|\Theta_{q,t}^{(i)} - \Theta_{q,0}^{(i)}\|^2 + \mathbb{E} \|\Theta_{q,0}^{(i)} - \Theta_{q,0}^{(i-1)}\|^2 + \dots + \mathbb{E} \|\Theta_{q,0}^{(2)} - \Theta_{q,0}^{(1)}\|^2 \\ &\stackrel{(b)}{=} \gamma^2 \mathbb{E} \left\| \sum_{s=1}^t \nabla_i f(x_{q,s-1}^{(i)}; \Theta_{q,s-1}^{(i)} \odot m_q^{(i)}) \right\|^2 + \gamma^2 \sum_{j=1}^{i-1} \mathbb{E} \left\| \sum_{t=1}^T \nabla_j f(x_{q,t-1}^{(j)}; \Theta_{q,t-1}^{(j)} \odot m_q^{(j)}) \right\|^2 \\ &\stackrel{(c)}{\leq} \gamma^2 \mathbb{E} \left\| \sum_{s=1}^t \nabla F(\Theta_{q,s-1}^{(i)} \odot m_q^{(i)}) \right\|^2 + \gamma^2 \sum_{j=1}^{i-1} \mathbb{E} \left\| \sum_{t=1}^T \nabla F(\Theta_{q,t-1}^{(j)} \odot m_q^{(j)}) \right\|^2 + i\gamma^2 \sigma^2 \end{aligned}$$

$$\begin{aligned}
& \stackrel{(d)}{\leq} t\gamma^2 \sum_{s=1}^t \mathbb{E} \|\nabla F(\Theta_{q,s-1}^{(i)} \odot m_q^{(i)})\|^2 + \gamma^2 T \sum_{j=1}^{i-1} \sum_{t=1}^T \mathbb{E} \|\nabla F(\Theta_{q,t-1}^{(j)} \odot m_q^{(j)})\|^2 + i\gamma^2 \sigma^2 \\
& \leq \gamma^2 T \sum_{j=1}^i \sum_{t=1}^T \mathbb{E} \|\nabla F(\Theta_{q,t-1}^{(j)} \odot m_q^{(j)})\|^2 + \kappa \gamma^2 \sigma^2 \\
& \leq 2\gamma^2 T \sum_{j=1}^i \sum_{t=1}^T \mathbb{E} \|\nabla F(\Theta_{q,t-1}^{(j)})\|^2 + 2\gamma^2 L^2 T \delta^2 \sum_{j=1}^i \sum_{t=1}^T \mathbb{E} \|\Theta_{q,0}^{(j)}\|^2 + \kappa \gamma^2 \sigma^2 \\
& = 2\gamma^2 T \sum_{j=1}^i \sum_{t=1}^T \mathbb{E} \|\nabla F(\Theta_{q,t-1}^{(j)})\|^2 + 2\gamma^2 L^2 T^2 \delta^2 \sum_{j=1}^i \mathbb{E} \|\Theta_{q,0}^{(j)}\|^2 + \kappa \gamma^2 \sigma^2
\end{aligned} \tag{28}$$

where (a) holds because $\Theta_{q,0}^{(i)} - \Theta_{q,0}^{(i-1)}$ and $\Theta_{q,0}^{(j)} - \Theta_{q,0}^{(j-1)}$ are orthogonal to each other when $i \neq j$, (b) holds because of (26) and (27), (c) holds because of Assumption 2, and (d) holds because of the Jensen's inequality. With the above inequality, it holds for $t \in [1, T]$ that

$$\begin{aligned}
\mathbb{E} \|\nabla_i F(\Theta_{q,0}^{(1)})\|^2 & \leq 2\mathbb{E} \|\nabla_i F(\Theta_{q,t}^{(i)})\|^2 + 2\mathbb{E} \|\nabla_i F(\Theta_{q,t}^{(i)}) - \nabla_i F(\Theta_{q,0}^{(1)})\|^2 \\
& \leq 2\mathbb{E} \|\nabla_i F(\Theta_{q,t}^{(i)})\|^2 + 2\mathbb{E} \|\nabla F(\Theta_{q,t}^{(i)}) - \nabla F(\Theta_{q,0}^{(1)})\|^2 \\
& \stackrel{(5)}{\leq} 2\mathbb{E} \|\nabla_i F(\Theta_{q,t}^{(i)})\|^2 + 2L^2 \mathbb{E} \|\Theta_{q,t}^{(i)} - \Theta_{q,0}^{(1)}\|^2 \\
& \stackrel{(28)}{\leq} 2\mathbb{E} \|\nabla_i F(\Theta_{q,t}^{(i)})\|^2 + 4L^2 \gamma^2 T \sum_{j=1}^i \sum_{t=1}^T \mathbb{E} \|\nabla F(\Theta_{q,t-1}^{(j)})\|^2 \\
& \quad + 4\gamma^2 L^4 T^2 \delta^2 \sum_{j=1}^i \mathbb{E} \|\Theta_{q,0}^{(j)}\|^2 + 2\kappa \gamma^2 \sigma^2 L^2
\end{aligned} \tag{29}$$

Summing the above inequality over $t = 0, 1, \dots, T$, we have

$$\begin{aligned}
T \mathbb{E} \|\nabla_i F(\Theta_{q,0}^{(1)})\|^2 & \leq 2 \sum_{t=1}^T \mathbb{E} \|\nabla_i F(\Theta_{q,t-1}^{(i)})\|^2 + 4T^2 L^2 \gamma^2 \sum_{j=1}^i \sum_{t=1}^T \mathbb{E} \|\nabla F(\Theta_{q,t-1}^{(j)})\|^2 \\
& \quad + 4\gamma^2 L^4 T^3 \delta^2 \sum_{j=1}^i \mathbb{E} \|\Theta_{q,0}^{(j)}\|^2 + 2\kappa \gamma^2 \sigma^2 L^2 T
\end{aligned} \tag{30}$$

Summing the above inequality over $i = 1, \dots, \kappa$, we have

$$\begin{aligned}
T \sum_{i=1}^{\kappa} \mathbb{E} \|\nabla_i F(\Theta_{q,0}^{(1)})\|^2 & \leq 2 \sum_{t=1}^T \sum_{i=1}^{\kappa} \mathbb{E} \|\nabla_i F(\Theta_{q,t-1}^{(i)})\|^2 + 4T^2 L^2 \gamma^2 \kappa \sum_{j=1}^{\kappa} \sum_{t=1}^T \mathbb{E} \|\nabla F(\Theta_{q,t-1}^{(j)})\|^2 \\
& \quad + 4\gamma^2 L^4 T^3 \delta^2 \kappa \sum_{j=1}^{\kappa} \mathbb{E} \|\Theta_{q,0}^{(j)}\|^2 + 2\kappa \gamma^2 \sigma^2 L^2 T \\
& = \left(4T^2 L^2 \gamma^2 \kappa + 2 \right) \sum_{t=1}^T \sum_{i=1}^{\kappa} \mathbb{E} \|\nabla_i F(\Theta_{q,t-1}^{(i)})\|^2 \\
& \quad + 4\gamma^2 L^4 T^3 \delta^2 \kappa \sum_{j=1}^{\kappa} \mathbb{E} \|\Theta_{q,0}^{(j)}\|^2 + 2\kappa \gamma^2 \sigma^2 L^2 T
\end{aligned} \tag{31}$$

Combining (24) and (31), we have

$$\begin{aligned}
T \sum_{i=1}^{\kappa} \mathbb{E} \|\nabla_i F(\Theta_{q,0}^{(1)})\|^2 & \\
& \leq \left(4T^2 L^2 \gamma^2 \kappa + 2 \right) \left(\frac{3}{\gamma} \left(\mathbb{E} [F(\Theta_{q,0}^{(1)}) - F(\Theta_{q+1,0}^{(1)})] \right) + \frac{3\gamma L \sigma^2 T \kappa}{2} + 2L^2 \delta^2 T \sum_{i=1}^{\kappa} \mathbb{E} \|\Theta_{q,0}^{(i)}\|^2 \right)
\end{aligned}$$

$$\begin{aligned}
& + 4\gamma^2 L^4 T^3 \delta^2 \kappa \sum_{i=1}^{\kappa} \mathbb{E} \|\Theta_{q,0}^{(i)}\|^2 + 2\kappa^2 \gamma^2 \sigma^2 L^2 T \\
& \stackrel{(a)}{\leq} \frac{12}{\gamma} \left(\mathbb{E}[F(\Theta_{q,0}^{(1)}) - F(\Theta_{q+1,0}^{(1)})] \right) + (6\gamma LT \kappa + 2\kappa^2 \gamma^2 L^2 T) \sigma^2 \\
& \quad + \left(4\gamma^2 L^4 T^3 \delta^2 \kappa + 8L^2 \delta^2 T \right) \sum_{i=1}^{\kappa} \mathbb{E} \|\Theta_{q,0}^{(i)}\|^2 \\
& \stackrel{(b)}{\leq} \frac{12}{\gamma} \left(\mathbb{E}[F(\Theta_{q,0}^{(1)}) - F(\Theta_{q+1,0}^{(1)})] \right) + 8\gamma LT \kappa \sigma^2 + 10L^2 \delta^2 T \sum_{i=1}^{\kappa} \mathbb{E} \|\Theta_{q,0}^{(i)}\|^2
\end{aligned} \tag{32}$$

where (a) and (b) use the facts that

$$2T^2 L^2 \gamma^2 \kappa + 1 \leq 2 \quad (\text{it is enough to set } \gamma \leq \frac{1}{\sqrt{2\kappa LT}}), \tag{33}$$

$$\kappa^2 \gamma^2 L^2 T \leq \gamma LT \kappa \quad (\text{it is enough to set } \gamma \leq \frac{1}{\kappa L}). \tag{34}$$

Then the inequality (32) becomes

$$\mathbb{E} \|\nabla F(\Theta_{q,0}^{(1)})\|^2 \leq \frac{12}{\gamma T} \left(\mathbb{E}[F(\Theta_{q,0}^{(1)}) - F(\Theta_{q+1,0}^{(1)})] \right) + 8\gamma L \kappa \sigma^2 + 10L^2 \delta^2 \sum_{i=1}^{\kappa} \mathbb{E} \|\Theta_{q,0}^{(i)}\|^2. \tag{35}$$

□

Finally we establish the convergence of the S-Gap algorithm as follows:

Theorem 1 (S-GAP CONVERGENCE). *Under Assumptions 1-3, if learning rate is set as $\gamma = \frac{1}{4\kappa LT \sqrt{Q}}$, it holds that*

$$\frac{1}{Q} \sum_{q=1}^Q \mathbb{E} \|\nabla F(\Theta_{q,0}^{(1)} \odot m_q^{(1)})\|^2 \leq \frac{G}{\sqrt{Q}} + \frac{10L^2 T \delta^2}{Q} \sum_{q=1}^Q \sum_{i=1}^{\kappa} \mathbb{E} \|\Theta_{q,0}^{(i)}\|^2 \tag{36}$$

where $G = 96\kappa L \mathbb{E}[F(\Theta_{1,0}^{(1)})] + \sigma^2$ is a constant.

Proof. Since

$$\mathbb{E} \|\nabla F(\Theta_{q,0}^{(1)} \odot m_q^{(1)})\|^2 \leq 2\mathbb{E} \|\nabla F(\Theta_{q,0}^{(1)})\|^2 + 2L^2 \delta^2 \mathbb{E} \|\Theta_{q,0}^{(1)}\|^2, \tag{37}$$

we thus have

$$\begin{aligned}
& \mathbb{E} \|\nabla F(\Theta_{q,0}^{(1)} \odot m_q^{(1)})\|^2 \\
& \stackrel{(25)}{\leq} \frac{24}{\gamma T} \left(\mathbb{E}[F(\Theta_{q,0}^{(1)}) - F(\Theta_{q+1,0}^{(1)})] \right) + 8L^2 T \delta^2 \sum_{i=1}^{\kappa} \mathbb{E} \|\Theta_{q,0}^{(i)}\|^2 + 4\gamma LT \kappa \sigma^2 + 2L^2 \delta^2 \mathbb{E} \|\Theta_{q,0}^{(1)}\|^2 \\
& \leq \frac{24}{\gamma T} \left(\mathbb{E}[F(\Theta_{q,0}^{(1)}) - F(\Theta_{q+1,0}^{(1)})] \right) + 10L^2 T \delta^2 \sum_{i=1}^{\kappa} \mathbb{E} \|\Theta_{q,0}^{(i)}\|^2 + 4\gamma LT \kappa \sigma^2
\end{aligned} \tag{38}$$

Summing the above inequality over $q = 1, \dots, Q$ and taking its average, we achieve

$$\frac{1}{Q} \sum_{q=1}^Q \|\nabla F(\Theta_{q,0}^{(1)} \odot m_q^{(1)})\|^2 \leq \frac{24}{\gamma T Q} \mathbb{E}[F(\Theta_{1,0}^{(1)})] + \frac{10L^2 T \delta^2}{Q} \sum_{q=1}^Q \sum_{i=1}^{\kappa} \mathbb{E} \|\Theta_{q,0}^{(i)}\|^2 + 4\gamma LT \kappa \sigma^2 \tag{39}$$

If we let $\gamma = \frac{1}{4\kappa LT \sqrt{Q}}$, the above inequalities becomes

$$\frac{1}{Q} \sum_{q=1}^Q \|\nabla F(\Theta_{q,0}^{(1)} \odot m_q^{(1)})\|^2 \leq \frac{96\kappa L}{\sqrt{Q}} \mathbb{E}[F(\Theta_{1,0}^{(1)})] + \frac{\sigma^2}{\sqrt{Q}} + \frac{10L^2 T \delta^2}{Q} \sum_{q=1}^Q \sum_{i=1}^{\kappa} \mathbb{E} \|\Theta_{q,0}^{(i)}\|^2 \tag{40}$$

which completes the proof.

□